

Local dynamical characteristics of Bessel beams upon reflection near the Brewster angle

Zhi-Wei Cui(崔志伟), Shen-Yan Guo(郭沈言), Yuan-Fei Hui(惠元飞)‡, Ju Wang(王举), and Yi-Ping Han(韩一平)
Citation: Chin. Phys. B, 2021, 30 (**4**): 044201. DOI: 10.1088/1674-1056/abd390
Journal homepage: http://cpb.iphy.ac.cn; http://iopscience.iop.org/cpb

What follows is a list of articles you may be interested in

A novel plasmonic refractive index sensor based on gold/silicon complementary grating structure

Xiangxian Wang(王向贤), Jiankai Zhu(朱剑凯), Yueqi Xu(徐月奇), Yunping Qi(祁云平), Liping Zhang(张丽萍), Hua Yang(杨华), and Zao Yi(易早)
Chin. Phys. B, 2021, 30 (**2**): 024207. DOI: 10.1088/1674-1056/abd690

A 3-kHz Er: YAG single-frequency laser with a ‘triple-reflection’ configuration on a piezoelectric actuator

Shuai Huang(黄帅), Qing Wang(王庆), Meng Zhang(张濛), Chaoyong Chen(陈朝勇), Kaixin Wang(王凯鑫), Mingwei Gao(高明伟), Chunqing Gao(高春清)
Chin. Phys. B, 2020, 29 (**8**): 084204. DOI: 10.1088/1674-1056/ab9441

Microwave frequency transfer over a 112-km urban fiber link based on electronic phase compensation

Wen-Xiang Xue(薛文祥), Wen-Yu Zhao(赵文宇), Hong-Lei Quan(全洪雷), Cui-Chen Zhao(赵粹臣), Yan Xing(邢燕), Hai-Feng Jiang(姜海峰), Shou-Gang Zhang(张首刚)
Chin. Phys. B, 2020, 29 (**6**): 064209. DOI: 10.1088/1674-1056/ab84d6

Generation of Mathieu beams using angular pupil modulation

Zhijun Ren(任志君), Jinping He(何晋平), Yile Shi(施逸乐)
Chin. Phys. B, 2018, 27 (**12**): 124201. DOI: 10.1088/1674-1056/27/12/124201

Generalization and propagation of spiraling Bessel beams with a helical axicon

Sun Qiong-Ge, Zhou Ke-Ya, Fang Guang-Yu, Liu Zheng-Jun, Liu Shu-Tian
Chin. Phys. B, 2012, 21 (**1**): 014208. DOI: 10.1088/1674-1056/21/1/014208

Local dynamical characteristics of Bessel beams upon reflection near the Brewster angle*

Zhi-Wei Cui(崔志伟)†, Shen-Yan Guo(郭沈言), Yuan-Fei Hui(惠元飞)‡, Ju Wang(王举), and Yi-Ping Han(韩一平)

School of Physics and Optoelectronic Engineering, Xidian University, Xi'an 710071, *China*

(Received 22 September 2020; revised manuscript received 23 October 2020; accepted manuscript online 15 December 2020)

We analytically and numerically study the local dynamical characteristics of the Bessel beams reflected from an air–glass interface near the Brewster angle. A Taylor series expansion based on the angular spectrum component is applied to correct the reflection coefficients near the Brewster angle. Using a hybrid angular spectrum representation and vector potential method, the explicit expressions for the electric and magnetic field components of the reflected Bessel beams are derived analytically under paraxial approximation. The local energy, momentum, spin, and orbital angular momentum of the Bessel beams upon reflection near the Brewster angle are examined numerically by utilizing a canonical approach. Numerical simulation results show that the properties of these dynamical quantities for the Bessel beams near Brewster angle incidence change abruptly, and are significantly affected by their topological charge, half-cone angle, and polarization state. The present study has its importance in understanding the dynamical aspects of optical beams with vortex structure and diffraction-free nature during the reflection process.

Keywords: Bessel beams, reflection, Brewster angle, momentum, angular momentum

PACS: 42.25.Gy, 42.60.Jf, 42.50.Tx **DOI:** 10.1088/1674-1056/abd390

1. Introduction

In recent years, a special type of light beams that do not spread on propagation, *i.e.* the so-called nondiffracting beams, has attracted much attention for its interesting properties and potential applications.[1–9] The best known example of such beams is the Bessel beams, which are the exact solutions of the Helmholtz wave equation in circular cylindrical coordinates and described by Bessel function of the first kind.[10–17] The intensity distributions of these beams exhibit circular symmetry and consist of a series of concentric rings. The zero-order Bessel beam has a high-intensity central core, whereas the higher-order Bessel beams have a dark central core. As a special type of electromagnetic waves, the nondiffracting Bessel beams can carry not only energy and momentum but also angular momentum, which includes the spin angular momentum (SAM) corresponding to the polarization of the beams and the orbital angular momentum (OAM) associated to the spatial distribution of the beams. It is well known that the energy, momentum, SAM, and OAM are the main dynamical characteristics of light and play a crucial role in the understanding of the light–matter interactions. Meanwhile, the reflection of light from an interface between two media with different material properties is a well-known phenomenon involving the light–matter interaction. The existing studies have shown that a bounded beam of light upon reflection near the Brewster angle exhibits a variety of interesting phenomena, such as large and negative Goos–Hänchen (GH) shift,[18] large in-plane angular shift,[19] and switchable and enhanced photonic spin Hall effect (PSHE).[20] It is expected that these phenomena accompanying the reflection of a beam at an interface near the Brewster angle will lead to the change of its energy, momentum, SAM, and OAM. Now a question arises: how do these dynamical quantities of the Bessel beams change upon reflection near the Brewster angle? The study on this issue could provide useful insights into the behavior of optical beams with vortex structure and diffraction-free nature during the reflection process, and find potential applications in the fields of new optical sensing, information processing, and new optoelectronic devices design.

There have been some studies on the reflection of Bessel beams at the interface between two media and the accompanying phenomena.[21–26] Mugnai first examined the behavior of a Bessel beam on total reflection;[21] however, only zero-order Bessel beam is considered. Later, Novitsky and Barkovsky further studied the total internal reflection of Bessel beams with arbitrary order and the accompanying IF shift.[22] Novitsky also studied the change of the size of Bessel beam rings under reflection.[23] Subsequently, Aiello and Woerdman discussed the GH and IF shifts of the Bessel beams upon reflection.[24] Brandão and Pires explored the reflection of vector Bessel beams at an interface between dielectrics.[25] More recently, Liu *et al.* analytically investigated the reflec-

*Project supported by the Natural Science Foundation of Shaanxi Province, China (Grant No. 2020JM-210) and the National Natural Science Foundation of China (Grant No. 61675159).

†Corresponding author. E-mail: zwcui@mail.xidian.edu.cn

‡Corresponding author. E-mail: yuanfeihuixd@163.com

© 2021 Chinese Physical Society and IOP Publishing Ltd

tion of a Bessel vortex beam incident on a uniaxial anisotropic media.[26] There have also been some reports on the dynamical properties of Bessel beams.[27–34] An analysis of the energy of Bessel beams was presented in Ref. [27]. The OAM density of higher-order Bessel beams was investigated in Refs. [28,29]. The coupling between SAM and OAM of the Bessel beams via spin–orbit interaction was studied in Refs. [30,32–34]. Despite all these works, few attentions have been paid to the energy, momentum, SAM, and OAM of the Bessel beams upon reflection. These dynamical quantities are of great importance in understanding the dynamical processes concerning the reflection of light beams. In this paper, we focus on the local dynamical characteristics of Bessel beams upon reflection near the Brewster angle. A Taylor series expansion based on the angular spectrum component[35] is used to correct the reflection coefficients near the Brewster angle that changes dramatically. A hybrid method based on the angular spectrum representation and vector potential in the Lorenz gauge[36] is introduced to derive the analytical expressions of the electric and magnetic field components of the reflected Bessel beams, which are the key to study their dynamical characteristics theoretically. The local energy, momentum, SAM, and OAM are described by using the canonical approach proposed by Bliokh *et al.*[37,38]

The rest of this paper is organized as follow. In Section 2, the theoretical formulae of this work are presented, where the explicit analytical expressions for the electric and magnetic field components of Bessel beams reflected at an air–medium interface are derived in detail. Some numerical simulations are performed and analyzed in Section 3. Finally, the conclusion is drawn in Section 4.

2. Theoretical formulae

2.1. Angular spectrum representation of the Bessel beams

In this section, we start with a description of the angular spectrum representation of the Bessel beams. As stated earlier, the Bessel beams are the exact solutions of the Helmholtz wave equation in circular cylindrical coordinates (ρ,ϕ,z). Mathematically, the scalar electric field of a Bessel beam propagating in the $+z$ direction is given by

$$E(\rho,\phi,z)=\mathrm{J}_l\left(k_\rho\rho\right)\exp(\mathrm{i}l\phi)\exp(\mathrm{i}k_z z), \tag{1}$$

where $\mathrm{J}_l(\cdot)$ is the Bessel function of the first kind, with l being the order numbers of the Bessel function. Here, l is also called the topological charge of phase singularities. The parameters $\rho=\sqrt{x^2+y^2}$ and $\phi=\tan^{-1}(y/x)$ are the radial distance and azimuthal angle in the transverse plane (x,y), respectively, $k_\rho=\sqrt{k_x^2+k_y^2}$ and $k_z=\sqrt{k^2-k_x^2-k_y^2}$ are the transversal and longitudinal components of the wavevectors k, respectively. Usually, these two components are more conveniently expressed as $k_\rho=k\sin\vartheta_0$ and $k_z=k\cos\vartheta_0$, with ϑ_0 being the half-cone angle of the Bessel beam. If $\sin\vartheta_0\ll 1$, the wavevectors $\boldsymbol{k}$ are almost parallel to the z axis and the transverse components (k_x,k_y) are small compared to k. In this case, the longitudinal component k_z can be expanded in a series as

$$k_z=\sqrt{k^2-k_x^2-k_y^2}\approx k-\frac{k_x^2+k_y^2}{2k}. \tag{2}$$

Under the above paraxial approximation, considering the relation $k_\rho^2=k_x^2+k_y^2$, equation (1) takes the form

$$E(\rho,\phi,z)=\mathrm{J}_l\left(k_\rho\rho\right)\exp(\mathrm{i}l\phi)\exp\left(-\mathrm{i}\frac{k_\rho^2}{2k}z\right)\exp(\mathrm{i}kz). \tag{3}$$

In this work we will consider, for simplicity, only the paraxial Bessel beams given by Eq. (3). By setting $z=0$, we obtain the complex amplitude of the Bessel beams in the initial plane

$$u(\rho,\phi,z=0)=\mathrm{J}_l\left(k_\rho\rho\right)\exp(\mathrm{i}l\phi). \tag{4}$$

Following the idea of angular spectrum representation, the Bessel beams can be expanded in terms of lots of plane waves with variable amplitudes and propagation directions. By taking the Fourier transform of Eq. (4), we can evaluate the angular spectrum amplitude of Bessel beams, as follows:[39]

$$\begin{aligned}\tilde{u}(\theta,\varphi)=&\frac{1}{4\pi^2}\int_0^\infty\int_0^{2\pi}u(\rho,\phi,z=0)\\&\times\exp[-\mathrm{i}kr\sin\theta\cos(\varphi-\phi)]\rho\,\mathrm{d}\rho\,\mathrm{d}\phi,\end{aligned} \tag{5}$$

where θ and φ being the spherical coordinates in k space.

Substituting Eq. (4) into Eq. (5), utilizing the following integral formula:[40]

$$\begin{aligned}&\int_0^{2\pi}\exp(\mathrm{i}l\varphi)\exp[-\mathrm{i}\rho\cos(\phi-\varphi)]\,\mathrm{d}\varphi\\&=2\pi\mathrm{i}^l\mathrm{J}_l(-\rho)\exp(\mathrm{i}l\phi),\end{aligned} \tag{6}$$

and recalling the properties of Dirac delta function[39]

$$\delta(b-a)=b\int_0^\infty r\mathrm{J}_l(br)\mathrm{J}_l(ar)\,\mathrm{d}r, \tag{7}$$

$$\delta(ax)=\frac{\delta(x)}{|a|},\quad \delta[g(x)]=\frac{\delta(x-x_0)}{|g'(x_0)|}, \tag{8}$$

it is finally derived that

$$\tilde{u}(\theta,\phi)=\frac{1}{2\pi\mathrm{i}^l}\frac{\delta(\theta-\vartheta_0)}{k^2\sin\vartheta_0\cos\vartheta_0}\exp(\mathrm{i}l\phi). \tag{9}$$

2.2. Vector wave analysis of the Bessel beams upon reflection

As a next step, we now consider the reflection of Bessel beams at a plane interface between air and a homogeneous glass. It is well known that the reflection of plane waves at an interface between two media is described by the Snell law and Fresnel formulas, which, however, are not accurately complied by the Bessel beams. As has been mentioned, Bessel

beams consist of a lot of plane waves, which are incident at different angles. Although each of the plane waves satisfies the Snell and Fresnel laws, their superposition exhibits unique polarization properties. To reveal some important and interesting features, it is necessary to carry out a vector wave analysis of the Bessel beams upon reflection. Here we adopt a hybrid method based on the angular spectrum representation and vector potential in the Lorenz gauge[36] to describe the vectorial structure of Bessel beams upon reflection.

Figure 1 schematically illustrates the reflection of a Bessel beam at an interface between two media. The beam is assumed to be incident from the air characterized by permittivity and permeability (ε_0, μ_0) to a homogeneous glass characterized by (ε_1, μ_1). A global coordinate system (x, y, z) is attached to the interface, in which the z axis is perpendicular to the interface located at $z = 0$. Two local coordinate systems $(x_\mathrm{i}, y_\mathrm{i}, z_\mathrm{i})$ and $(x_\mathrm{r}, y_\mathrm{r}, z_\mathrm{r})$, corresponding to two cylindrical coordinate systems $(\rho_\mathrm{i}, \phi_\mathrm{i}, z_\mathrm{i})$ and $(\rho_\mathrm{r}, \phi_\mathrm{r}, z_\mathrm{r})$, are used to describe the incident and reflected Bessel beams, respectively. The angles ϑ_i and ϑ_r denote the incident angle and reflection angle of the main Fourier component, respectively.

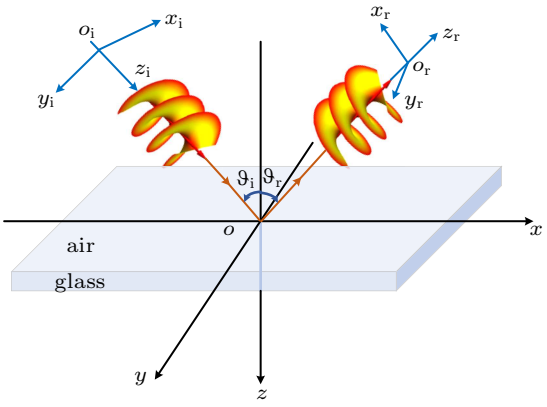


Fig. 1. Illustration of a Bessel beam reflected from an air–glass interface.

In the coordinate system $(x_\mathrm{i}, y_\mathrm{i}, z_\mathrm{i})$, an arbitrarily polarized Bessel beam is assumed to propagate parallel to the positive z_i axis, the vector potential of such a beam can be expressed as

$$\boldsymbol{A}_\mathrm{i} = (\alpha\hat{\boldsymbol{x}}_\mathrm{i} + \beta\hat{\boldsymbol{y}}_\mathrm{i})\, u_\mathrm{i} \exp(\mathrm{i}k_\mathrm{i} z_\mathrm{i}), \tag{10}$$

where the parameters α and β satisfying $|\alpha|^2 + |\beta|^2 = 1$ determine the polarization state of the incident beam, $k_\mathrm{i} = k_0 = 2\pi/\lambda_0$ is the wave number in the air, with λ_0 being the wavelength of the beam, and u_i is the complex amplitude of the Bessel beam. Within the paraxial approximation, the two dimensional Fourier transform of the complex amplitude u_i takes the form[39]

$$\begin{aligned} u_\mathrm{i} = & \int_0^\infty \int_0^{2\pi} \tilde{u}_\mathrm{i} \exp[\mathrm{i}k_\mathrm{i}\rho_\mathrm{i} \sin\theta_\mathrm{i} \cos(\phi_\mathrm{i} - \varphi_\mathrm{i})] \\ & \times \exp\left(-\mathrm{i}\frac{k_\mathrm{i} \sin^2\theta_\mathrm{i}}{2} z_\mathrm{i}\right) k_\mathrm{i}^2 \cos\theta_\mathrm{i} \sin\theta_\mathrm{i} \mathrm{d}\theta_\mathrm{i} \mathrm{d}\phi_\mathrm{i}, \end{aligned} \tag{11}$$

with

$$\tilde{u}_\mathrm{i} = \frac{1}{2\pi \mathrm{i}^l} \frac{\delta(\theta_\mathrm{i} - \vartheta_0)}{k_\mathrm{i}^2 \sin\vartheta_0 \cos\vartheta_0} \exp(\mathrm{i}l\phi_\mathrm{i}), \tag{12}$$

being the angular spectrum of the Bessel beam. As we can see, a Bessel beam has been decomposed into lots of plane waves, which can be used to analyze the Bessel beam reflection at an interface between two different dielectric media.

After reflection of the Bessel beam from an air–glass interface, the corresponding vector potential in the coordinate system $(x_\mathrm{r}, y_\mathrm{r}, z_\mathrm{r})$ can be written as

$$A_\mathrm{r} = \left(u_\mathrm{r}^\mathrm{H} \hat{x}_\mathrm{r} + u_\mathrm{r}^\mathrm{V} \hat{y}_\mathrm{r}\right) \exp(\mathrm{i}k_\mathrm{r} z_\mathrm{r}), \tag{13}$$

where $k_\mathrm{r} = k_0$, u_r^H and u_r^V are the transverse amplitudes of the reflected Bessel beam, which can be evaluated by

$$\begin{aligned} \begin{bmatrix} u_\mathrm{r}^\mathrm{H} \\ u_\mathrm{r}^\mathrm{V} \end{bmatrix} = & \int_0^\infty \int_0^{2\pi} \begin{bmatrix} \tilde{u}_\mathrm{r}^\mathrm{H} \\ \tilde{u}_\mathrm{r}^\mathrm{V} \end{bmatrix} \exp[\mathrm{i}k_\mathrm{r}\rho_\mathrm{r} \sin\theta_\mathrm{r} \cos(\phi_\mathrm{r} - \varphi_\mathrm{r})] \\ & \times \exp\left(-\mathrm{i}\frac{k_\mathrm{r} \sin^2\theta_\mathrm{r}}{2} z_\mathrm{r}\right) k_\mathrm{r}^2 \cos\theta_\mathrm{r} \sin\theta_\mathrm{r} \mathrm{d}\theta_\mathrm{r} \mathrm{d}\phi_\mathrm{r}, \end{aligned} \tag{14}$$

with $\tilde{u}_\mathrm{r}^\mathrm{H}$ and $\tilde{u}_\mathrm{r}^\mathrm{V}$ being the horizontal and vertical components of the angular spectra for the reflected beam, respectively. Following the works of Luo *et al.*,[20,41,42] we can express the angular spectra $\tilde{u}_\mathrm{r}^\mathrm{H}$ and $\tilde{u}_\mathrm{r}^\mathrm{V}$ as

$$\begin{bmatrix} \tilde{u}_\mathrm{r}^\mathrm{H} \\ \tilde{u}_\mathrm{r}^\mathrm{V} \end{bmatrix} = \begin{bmatrix} r_\mathrm{p} & \dfrac{k_{\mathrm{r}y}(r_\mathrm{p} + r_\mathrm{s}) \cot\vartheta_\mathrm{i}}{k_0} \\ -\dfrac{k_{\mathrm{r}y}(r_\mathrm{p} + r_\mathrm{s}) \cot\vartheta_\mathrm{i}}{k_0} & r_\mathrm{s} \end{bmatrix} \begin{bmatrix} \tilde{u}_\mathrm{i}^\mathrm{H} \\ \tilde{u}_\mathrm{i}^\mathrm{V} \end{bmatrix}, \tag{15}$$

where $\tilde{u}_\mathrm{i}^\mathrm{H} = \alpha\tilde{u}_\mathrm{r}$ and $\tilde{u}_\mathrm{i}^\mathrm{V} = \beta\tilde{u}_\mathrm{r}$ with $\tilde{u}_\mathrm{r} = \tilde{u}_\mathrm{i}(-k_{\mathrm{r}x}, k_{\mathrm{r}y})$, r_p and r_s are the Fresnel reflection coefficients, which are explicitly given as

$$\begin{aligned} r_\mathrm{p} &= \frac{n^2 \cos\vartheta_\mathrm{i} - \sqrt{n^2 - \sin^2\vartheta_\mathrm{i}}}{n^2 \cos\vartheta_\mathrm{i} + \sqrt{n^2 - \sin^2\vartheta_\mathrm{i}}}, \\ r_\mathrm{s} &= \frac{\cos\vartheta_\mathrm{i} - \sqrt{n^2 - \sin^2\vartheta_\mathrm{i}}}{\cos\vartheta_\mathrm{i} + \sqrt{n^2 - \sin^2\vartheta_\mathrm{i}}}, \end{aligned} \tag{16}$$

in which, n denotes the refractive index of the homogeneous glass, the subscripts p and s identify the parallel and perpendicular polarizations, respectively. The existing studies have shown that the reflection coefficients change abruptly when the beam is incident near the Brewster angle and a Taylor series expansion based on the angular spectrum component could be utilized to correct the reflection coefficients.[20,43] In particular, r_p and r_s can be expanded as

$$r_{\mathrm{p,s}} = r_{\mathrm{p,s}} \left[1 - \frac{k_{\mathrm{r}x}}{k_0} \frac{\partial r_{\mathrm{p,s}}}{\partial \vartheta_\mathrm{i}}\right], \tag{17}$$

with k_{rx} being the component of the wavevector $\boldsymbol{k}_r$ in the angular spectrum space. By inserting Eq. (17) into Eq. (15) and neglecting the second order item we arrive at

$$\begin{bmatrix} \tilde{u}_r^H \\ \tilde{u}_r^V \end{bmatrix} = \begin{bmatrix} r_p\left(1-\dfrac{k_{rx}}{k_0}\dfrac{\partial r_p}{\partial \vartheta_i}\right) & \dfrac{k_{ry}\left(r_p+r_s\right)\cot\vartheta_i}{k_0} \\ -\dfrac{k_{ry}\left(r_p+r_s\right)\cot\vartheta_i}{k_0} & r_s\left(1-\dfrac{k_{rx}}{k_0}\dfrac{\partial r_s}{\partial \vartheta_i}\right) \end{bmatrix} \begin{bmatrix} \alpha\tilde{u}_r \\ \beta\tilde{u}_r \end{bmatrix}. \quad (18)$$

Before proceeding further, note that, the boundary conditions $k_{rx}=-k_{ix}$ and $k_{ry}=k_{iy}$ have been applied in Eqs. (15) and (17). Further considering the relations

$$\begin{aligned} &k_{i(r)x} = k_{i(r)}\sin\theta_{i(r)}\cos\varphi_{i(r)}, \\ &k_{i(r)y} = k_{i(r)}\sin\theta_{i(r)}\sin\varphi_{i(r)}, \\ &\exp\left[\mathrm{i}l\varphi_{i(r)}\right] = \left[\cos\varphi_{i(r)}+\mathrm{i}\sin\varphi_{i(r)}\right]^l. \end{aligned} \quad (19)$$

We can also write the reflection boundary conditions for the Bessel beams as

$$\theta_i = \theta_r, \exp\left(\mathrm{i}l\phi_i\right) = (-1)^l\exp\left(-\mathrm{i}l\phi_r\right). \quad (20)$$

Consequently, the angular spectrum amplitude of the Bessel beams after applying the reflection boundary conditions takes the form

$$\tilde{u}_r = \frac{1}{2\pi i^l}\frac{\delta\left(\theta_r-\vartheta_0\right)}{k_r^2\sin\vartheta_0\cos\vartheta_0}(-1)^l\exp\left(-\mathrm{i}l\phi_r\right). \quad (21)$$

The transverse amplitude u_r^H and u_r^V of the reflected Bessel beam can be calculated by substituting Eqs. (18) and (21) into Eq. (14). First, integration along θ_r is performed by recalling the properties of Dirac delta function given by Eqs. (7) and (8). Then, integration along ϕ_r is done by utilizing the following integral formula

$$\begin{aligned} &\int_0^{2\pi}\begin{bmatrix}\cos\varphi \\ \sin\varphi\end{bmatrix}\mathrm{e}^{-\mathrm{i}l\varphi}\,\mathrm{e}^{\mathrm{i}\rho\cos(\varphi-\phi)}\,\mathrm{d}\phi \\ &=\pi\begin{bmatrix} \mathrm{i}^{l+1}\mathrm{e}^{-\mathrm{i}(l+1)\phi}\mathrm{J}_{l+1}(\rho)+\mathrm{i}^{l-1}\mathrm{e}^{-\mathrm{i}(l-1)\phi}\mathrm{J}_{l-1}(\rho) \\ \mathrm{i}\cdot\mathrm{i}^{l+1}\mathrm{e}^{-\mathrm{i}(l+1)\phi}\mathrm{J}_{l+1}(\rho)-\mathrm{i}\cdot\mathrm{i}^{l-1}\mathrm{e}^{-\mathrm{i}(l-1)\phi}\mathrm{J}_{l-1}(\rho)\end{bmatrix}. \end{aligned} \quad (22)$$

After calculations, we obtain

$$u_r^H = \alpha r_p I_1 - \alpha r_p\frac{1}{k_0}\frac{\partial r_p}{\partial\vartheta_i}I_2 + \beta\frac{\left(r_p+r_s\right)\cot\vartheta_i}{k_0}I_3, \quad (23)$$

$$u_r^V = \beta r_s I_1 - \beta r_s\frac{1}{k_0}\frac{\partial r_s}{\partial\vartheta_i}I_2 - \alpha\frac{\left(r_p+r_s\right)\cot\vartheta_i}{k_0}I_3, \quad (24)$$

in which

$$I_1 = \mathrm{J}_l\left(k_{\rho r}\rho_r\right)(-1)^l\exp\left(-\mathrm{i}l\phi_r\right)\exp\left(-\mathrm{i}\frac{k_{\rho r}^2 z_r}{2k_r}\right), \quad (25)$$

$$I_2 = \left[-\frac{l\left(\mathrm{i}x_r-y_r\right)}{\rho_r^2}+\frac{\mathrm{i}k_{\rho r}x_r}{\rho_r}\frac{\mathrm{J}_{l+1}\left(k_{\rho r}\rho_r\right)}{\mathrm{J}_l\left(k_{\rho r}\rho_r\right)}\right]I_1, \quad (26)$$

$$I_3 = \left[-\frac{l\left(x_r+\mathrm{i}y_r\right)}{\rho_r^2}+\frac{\mathrm{i}k_{\rho r}y_r}{\rho_r}\frac{\mathrm{J}_{l+1}\left(k_{\rho r}\rho_r\right)}{\mathrm{J}_l\left(k_{\rho r}\rho_r\right)}\right]I_1, \quad (27)$$

with $k_{\rho r}=k_r\sin\vartheta_0$, $\rho_r=\sqrt{x_r^2+y_r^2}$, and $\phi_r=\tan^{-1}\left(y_r/x_r\right)$.

Once the vector potential is obtained, the electric and magnetic field vectors of the reflected Bessel beam can be expressed in terms of $\boldsymbol{A}_r$ as

$$\boldsymbol{E}_r = \mathrm{i}k_r Z_r\boldsymbol{A}_r + \mathrm{i}\frac{Z_r}{k_r}\nabla\left(\nabla\cdot\boldsymbol{A}_r\right), \quad (28)$$

$$\boldsymbol{H}_r = \nabla\times\boldsymbol{A}_r, \quad (29)$$

where k_r and Z_r are wave number and wave impedance in the air, respectively. Then, inserting Eq. (13) to Eqs. (28) and (29), and making paraxial approximation, we have

$$E_r = \mathrm{i}k_r Z_r\left[u_r^H\hat{x}_r+u_r^V\hat{y}_r+\frac{\mathrm{i}}{k_r}\left(\frac{\partial u_r^H}{\partial x_r}+\frac{\partial u_r^V}{\partial y_r}\right)\hat{z}_r\right]\exp\left(\mathrm{i}k_r z_r\right), \quad (30)$$

$$H_r = \mathrm{i}k_r\left[-u_r^V\hat{x}_r+u_r^H\hat{y}_r-\frac{\mathrm{i}}{k_r}\left(\frac{\partial u_r^V}{\partial x_r}-\frac{\partial u_r^H}{\partial y_r}\right)\hat{z}_r\right]\exp\left(\mathrm{i}k_r z_r\right), \quad (31)$$

where $\partial u_r^H/\partial x_r$, $\partial u_r^V/\partial x_r$, $\partial u_r^H/\partial y_r$, and $\partial u_r^V/\partial y_r$ are given by

$$\frac{\partial u_r^H}{\partial x_r} = \alpha r_p\frac{\partial I_1}{\partial x_r}-\alpha r_p\frac{1}{k_0}\frac{\partial r_p}{\partial\vartheta_i}\frac{\partial I_2}{\partial x_r}+\beta\frac{\left(r_p+r_s\right)\cot\vartheta_i}{k_0}\frac{\partial I_3}{\partial x_r}, \quad (32)$$

$$\frac{\partial u_r^H}{\partial y_r} = \alpha r_p\frac{\partial I_1}{\partial y_r}-\alpha r_p\frac{1}{k_0}\frac{\partial r_p}{\partial\vartheta_i}\frac{\partial I_2}{\partial y_r}+\beta\frac{\left(r_p+r_s\right)\cot\vartheta_i}{k_0}\frac{\partial I_3}{\partial y_r}, \quad (33)$$

$$\frac{\partial u_r^V}{\partial x_r} = \beta r_s\frac{\partial I_1}{\partial x_r}-\beta r_s\frac{1}{k_0}\frac{\partial r_s}{\partial\vartheta_i}\frac{\partial I_2}{\partial x_r}-\alpha\frac{\left(r_p+r_s\right)\cot\vartheta_i}{k_0}\frac{\partial I_3}{\partial x_r}, \quad (34)$$

$$\frac{\partial u_r^V}{\partial y_r} = \beta r_s\frac{\partial I_1}{\partial y_r}-\beta r_s\frac{1}{k_0}\frac{\partial r_s}{\partial\vartheta_i}\frac{\partial I_2}{\partial y_r}-\alpha\frac{\left(r_p+r_s\right)\cot\vartheta_i}{k_0}\frac{\partial I_3}{\partial y_r}, \quad (35)$$

in which

$$\frac{\partial I_1}{\partial x_r} = \left[\frac{l\left(x_r+\mathrm{i}y_r\right)}{\rho_r^2}-\frac{k_{\rho r}x_r}{\rho_r}\frac{\mathrm{J}_{l+1}\left(k_{\rho r}\rho_r\right)}{\mathrm{J}_l\left(k_{\rho r}\rho_r\right)}\right]I_1, \quad (36)$$

$$\frac{\partial I_1}{\partial y_r} = \left[\frac{l\left(y_r-\mathrm{i}x_r\right)}{\rho_r^2}-\frac{k_{\rho r}y_r}{\rho_r}\frac{\mathrm{J}_{l+1}\left(k_{\rho r}\rho_r\right)}{\mathrm{J}_l\left(k_{\rho r}\rho_r\right)}\right]I_1, \quad (37)$$

$$\begin{aligned}\frac{\partial I_2}{\partial x_r} = &\left[\frac{\mathrm{i}l\left(l-1\right)\left(y_r-\mathrm{i}x_r\right)^2}{\rho_r^4}+\frac{\mathrm{i}k_{\rho r}^2x_r^2}{\rho_r^2}\right. \\ &\left.+\frac{\mathrm{i}k_{\rho r}\left(y_r^2-x_r^2+\mathrm{i}2lx_ry_r\right)}{\rho_r^3}\frac{\mathrm{J}_{l+1}(k_{\rho r}\rho_r)}{\mathrm{J}_l(k_{\rho r}\rho_r)}\right]I_1, \end{aligned} \quad (38)$$

$$\begin{aligned}\frac{\partial I_2}{\partial y_r} = &\left[\frac{l\left(l-1\right)\left(y_r-\mathrm{i}x_r\right)^2}{\rho_r^4}+\frac{\mathrm{i}k_{\rho r}^2x_ry_r}{\rho_r^2}\right. \\ &\left.+\frac{k_{\rho r}\left(lx_r^2-ly_r^2-\mathrm{i}2x_ry_r\right)}{\rho_r^3}\frac{\mathrm{J}_{l+1}(k_{\rho r}\rho_r)}{\mathrm{J}_l(k_{\rho r}\rho_r)}\right]I_1, \end{aligned} \quad (39)$$

$$\begin{aligned}\frac{\partial I_3}{\partial x_r} = &\left[\frac{l\left(l-1\right)\left(y_r-\mathrm{i}x_r\right)^2}{\rho_r^4}+\frac{\mathrm{i}k_{\rho r}^2x_ry_r}{\rho_r^2}\right. \\ &\left.+\frac{k_{\rho r}\left(lx_r^2-ly_r^2-\mathrm{i}2x_ry_r\right)}{\rho_r^3}\frac{\mathrm{J}_{l+1}(k_{\rho r}\rho_r)}{\mathrm{J}_l(k_{\rho r}\rho_r)}\right]I_1, \end{aligned} \quad (40)$$

$$\begin{aligned}\frac{\partial I_3}{\partial y_r} = &\left[\frac{\mathrm{i}l\left(l-1\right)\left(x_r+\mathrm{i}y_r\right)^2}{\rho_r^4}+\frac{\mathrm{i}k_{\rho r}^2y_r^2}{\rho_r^2}\right. \\ &\left.+\frac{\mathrm{i}k_{\rho r}\left(x_r^2-y_r^2-\mathrm{i}2lx_ry_r\right)}{\rho_r^3}\frac{\mathrm{J}_{l+1}(k_{\rho r}\rho_r)}{\mathrm{J}_l(k_{\rho r}\rho_r)}\right]I_1. \end{aligned} \quad (41)$$

2.3. Description of the energy, momentum, SAM, and OAM

Having written explicitly the analytical expressions of the electric and magnetic fields of the reflected Bessel beams, we now proceed to study the local energy, momentum, SAM, and OAM of the Bessel beams during the reflection process at the Brewster angle. Here we adopt a canonical approach proposed by Bliokh *et al.*[38] to describe these dynamical quantities. Specifically, the energy, canonical momentum, SAM, and OAM densities of the reflected Bessel beams can be expressed as

$$W = \frac{1}{4}\left(\varepsilon_0 |\boldsymbol{E}_{\rm r}|^2 + \mu_0 |\boldsymbol{H}_{\rm r}|^2\right), \tag{42}$$

$$\boldsymbol{P} = \frac{1}{4\omega}\,{\rm Im}\left[\varepsilon_0 \boldsymbol{E}_{\rm r}^* \cdot (\nabla)\,\boldsymbol{E}_{\rm r} + \mu_0 \boldsymbol{H}_{\rm r}^* \cdot (\nabla)\,\boldsymbol{H}_{\rm r}\right], \tag{43}$$

$$\boldsymbol{S} = \frac{1}{4\omega}\,{\rm Im}\left(\varepsilon_0 \boldsymbol{E}_{\rm r}^* \times \boldsymbol{E}_{\rm r} + \mu_0 \boldsymbol{H}_{\rm r}^* \times \boldsymbol{H}_{\rm r}\right), \tag{44}$$

$$\boldsymbol{L} = \boldsymbol{r} \times \boldsymbol{P}, \tag{45}$$

where ω is the angular frequency, ${\rm Im}[\cdot]$ denotes the imaginary parts, and the superscript "*" denotes the complex conjugate. Obviously, the momentum, SAM, and OAM densities are vectors that include the x, y, and z components. Usually, we consider the transverse and longitudinal components of these dynamical quantities separately. Here the transverse component includes the contributions of x and y components, and the longitudinal component is the z component.

3. Numerical results and discussion

In this section, we perform some numerical simulations to explore the local dynamical characteristics of the paraxial Bessel beams reflection at an interface between air and BK7 glass with refractive index $n = 1.515$, which leads to a Brewster angle $\theta_{\rm B} = 56.5°$. Besides the parameters given below every figure, the common parameters are chosen as: the free space wavelength of Bessel beams $\lambda_0 = 632.8$ nm, the half-cone angle $\vartheta_0 = 5°$, the polarization parameters $(\alpha, \beta) = (1, 0)$, *i.e.*, x linear polarization, the topological charge $l = 2$, and the position of observed plane $z_{\rm r} = \lambda_0$.

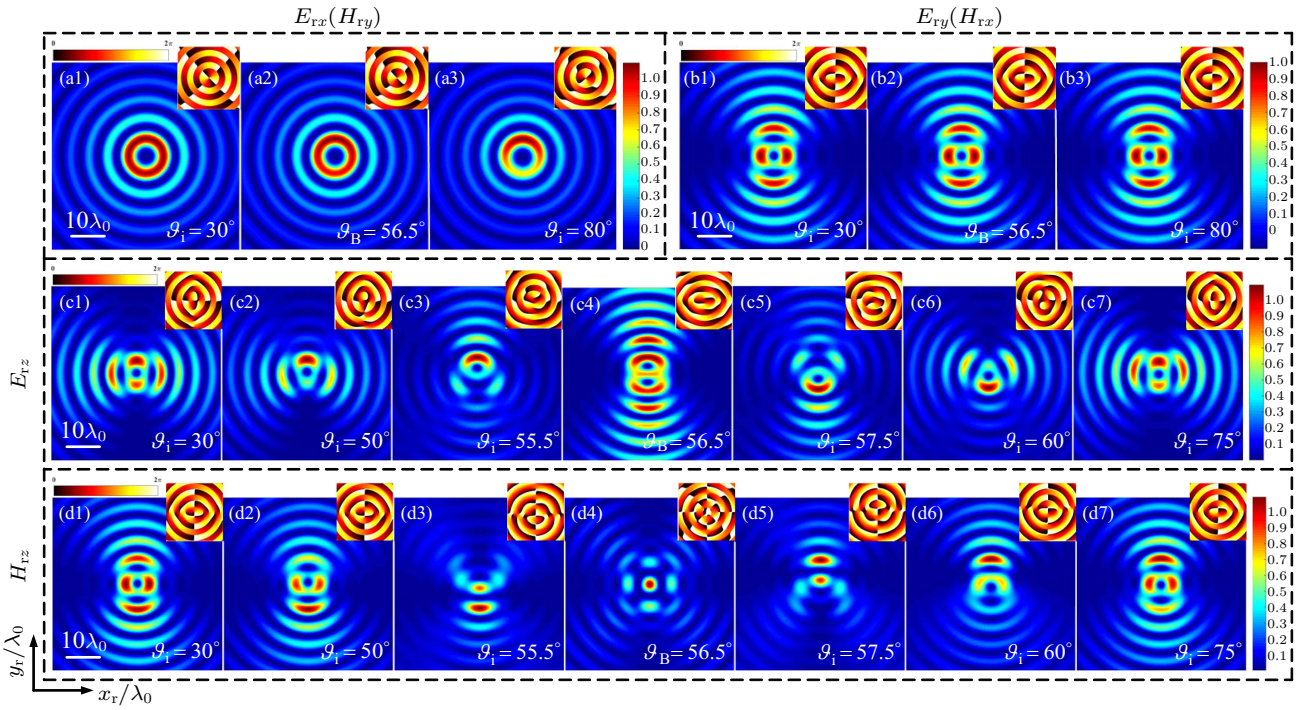


Fig. 2. Intensity patterns of the electric and magnetic field components of the reflected Bessel beams with different incident angles, and their corresponding phases are plotted in the upper right insets. Results are normalized to the corresponding maximum value of the total intensity for each illumination mode.

To start, we consider the field and phase distributions of the reflected Bessel beams with different incident angles. By comparing Eqs. (30) and (31), we find that $E_{rx} = Z_{\rm r} H_{\rm ry}$ and $E_{\rm ry} = -Z_{\rm r} H_{\rm rx}$, which indicate that E_{rx} and $H_{\rm ry}$, as well as $E_{\rm ry}$ and H_{rx} exhibit similar intensity patterns with different amplitudes. Here we only consider the components E_{rx}, $E_{\rm ry}$, $E_{\rm rz}$, and $H_{\rm rz}$. Figure 2 depicts the intensity patterns of these filed components, with their corresponding phases shown as insets in the top right corners. As is well known, the intensity distribution of the Bessel beams exhibits circular symmetry. For the incident Bessel beam with polarization parameters $(\alpha, \beta) = (1, 0)$, *i.e.*, x-linear polarization, its x component of the electric field and the y component of the magnetic field also possess circular symmetry. However, the intensity patterns of the central ring of the transverse field components E_{rx} and $H_{\rm ry}$ deviate from the circular symmetry. The distortions become more severe with the increasing of incident angle, as illustrated in Figs. 2(a1)–2(a3). When the incident angle is greater

than the Brewster angle, distortions lead to the loss of vortex phase properties in the reflected Bessel beams. It is worthy to note that the amplitude distributions of the transverse field components E_{ry} and H_{rx} induced by the cross-polarization during the reflection process almost do not change with increasing the incident angle, as illustrated in Figs. 2(b1)–2(b3). In contrast, the longitudinal field components E_{rz} and H_{rz} of the reflected Bessel beam are extremely sensitive to the incident angle, as shown in Figs. 2(c1)–2(c7) and Figs. 2(d1)–2(d7). It can be observed that the amplitude distributions of E_{rz} and H_{rz} at Brewster angle incidence change abruptly. When the incident angle increases or decreases by the same angle relative to Brewster angle, the intensity patterns of E_{rz} and H_{rz} are similar but rotate 180 degrees, which will lead to the change of the energy, momentum, SAM, and OAM of the reflected Bessel beam.

Next, we examine the influence of the incidence angle on the energy, momentum, SAM, and OAM densities of the Bessel beams upon reflection, as illustrated in Fig. 3. As we can see, the distribution patterns of these dynamical quantities for the reflected Bessel beams are sensitive to the incidence angle. Notably, the energy, momentum, SAM, and OAM change abruptly when the beam is incident near the Brewster angle. It can be seen that the distribution patterns of the energy and momentum densities for the reflected beams are similar except those near the Brewster angle. As the increase of the incident angle, the patterns gradually deviate from the circular symmetry. When the beam is incident near the Brewster angle, the circular symmetry of the patterns is seriously broken. Compared with the energy and momentum densities, the SAM density distribution of the reflected Bessel beam has completely lost the circular symmetry. Notably, when the incident angle increases or decreases by the same angle relative to Brewster angle, the distribution pattern of the SAM density remains unchanged. It also can be seen that the circular symmetry of the OAM density distribution pattern will be distorted as the incident angle increase. The distortions become much more serious when the incident angle is close to the Brewster angle.

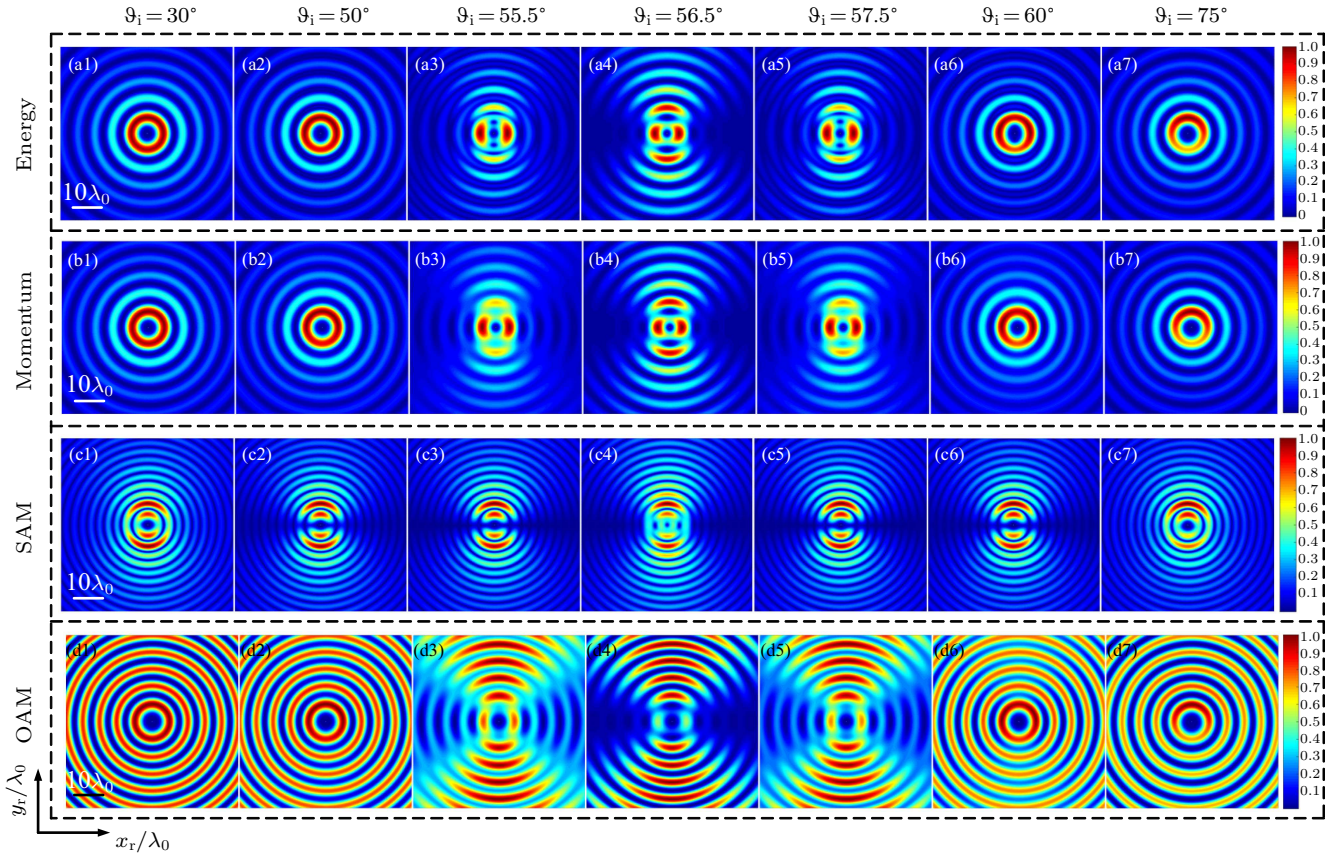


Fig. 3. Normalized energy, momentum, SAM, and OAM density distributions of the reflected Bessel beams with different incident angles. The first line to the last line corresponds to the energy, momentum, SAM, and OAM densities, respectively.

We now turn our attention to the local dynamical characteristics of Bessel beams upon reflection at the Brewster angle. Since the local energy and momentum densities of the reflected Bessel beams show similar characteristics, here we are only interested in the momentum, SAM, and OAM densities. Figure 4 illustrates the distributions of the transverse and longitudinal momentum, SAM and OAM densities of the reflected Bessel beams with different topological charges. From the illustrations of this figure, we observed that the momentum, SAM, and OAM densities have not only transverse com-

ponent but also longitudinal component due to the cross polarization effects accompanying the reflection. Further observation, we find that the change of the sign of the topological charge (from $l=-1$ to $l=1$, or *vice versa*) induces the change of the orientation of the transverse momentum density with its amplitude unchanging, whereas the longitudinal momentum has no alteration. At the same time, it is clear that the change of the sign of the topological charge has no effect on the transverse SAM and OAM, but has a significant effect on the longitudinal SAM and OAM. In particular, the longitudinal OAM density reverses from positive $(l=-1)$ to negative $(l=1)$ with changing the sign of the topological charge. It should be noted that the reflection boundary conditions, as represented by Eq. (20), induce the inverse of vortex phase rotation direction. It can also be seen in Fig. 4 that with the increasing of topological charge, the distributions of the momentum, SAM, and OAM densities gradually go away from the center. Moreover, we note that the longitudinal OAM for the case of $l=0$ is obviously different from that of $l\neq 0$. The above results show that altering the sign and value of the topological charge of the incident Bessel beam provides an effective way to regulate its local dynamical characteristics during the reflection process.

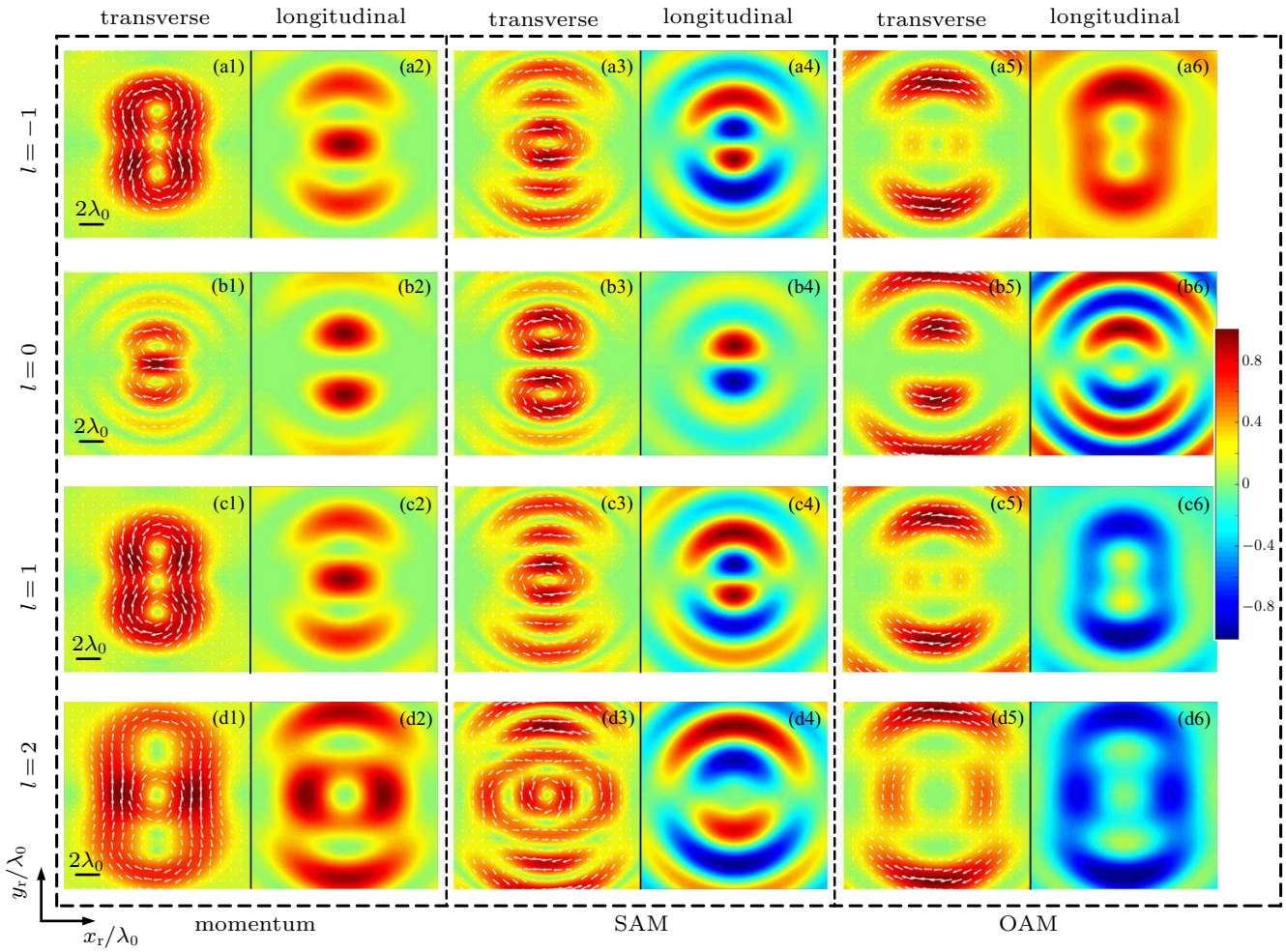


Fig. 4. Distributions of the transverse and longitudinal momentums, SAM, and OAM densities of the reflected Bessel beams with topological charges: (a1)–(a6) $l=-1$, (b1)–(b6) $l=0$, (c1)–(c6) $l=1$, and (d1)–(d6) $l=2$, where the white arrows show the orientations of their corresponding transverse components. Results are normalized to the corresponding maximum value of each subgraph.

Figure 5 shows the momentum, SAM, and OAM density distributions of reflected Bessel beams with different half-cone angles. As stated before, we restrict ourselves to the analysis of the reflection of the Bessel beams under paraxial approximation. Here we choose the half-cone angle as $\vartheta_0=5^\circ$, 10°, 15°. It can be seen from Fig. 5 that, the half-cone angle has a significant effect on the distributions of the momentum, SAM, and OAM densities. In particular, as the half-cone angle of the Bessel beam increases, the momentum, SAM, and OAM densities of the reflected beam gradually concentrate on the central area at the same observation plane. In addition, the larger the half-cone angle ϑ_0, the larger the amplitude of these of these dynamical quantities.

In all the numerical simulations above, the incident Bessel beams are assumed to be linearly polarized. As well known, the polarization state of a light beam can take different forms such as linear, circular, radial, azimuthal, and so on. Among which, the state of circular polarization is associated with SAM. It raises an interesting question, that is, how the local momentums, SAM, and OAM of the reflected beam be-

have when the incident Bessel beam is circularly polarized. To answer this question, we plot the distributions of the transverse and longitudinal momentums, SAM, and OAM densities for the Bessel beams with left circular polarization during the reflection process, as shown in Fig. 6. Comparing Fig. 6 with Figs. 4(d1)–4(d6), we find that the distribution patters of the local momentum, transverse SAM, and OAM densities change from axisymmetric structure to multi ring structure. The longitudinal SAM distribution of the linearly polarized Bessel beam is similar to that of the circularly polarized Bessel beam. We also find that both the momentum and SAM densities are mainly dominated by the longitudinal component of them, whereas the OAM density is dominated by its transverse component. This analysis suggests that changing the incident polarization offers an alternative way to regulate the local dynamical characteristics of Bessel beams during the reflection process.

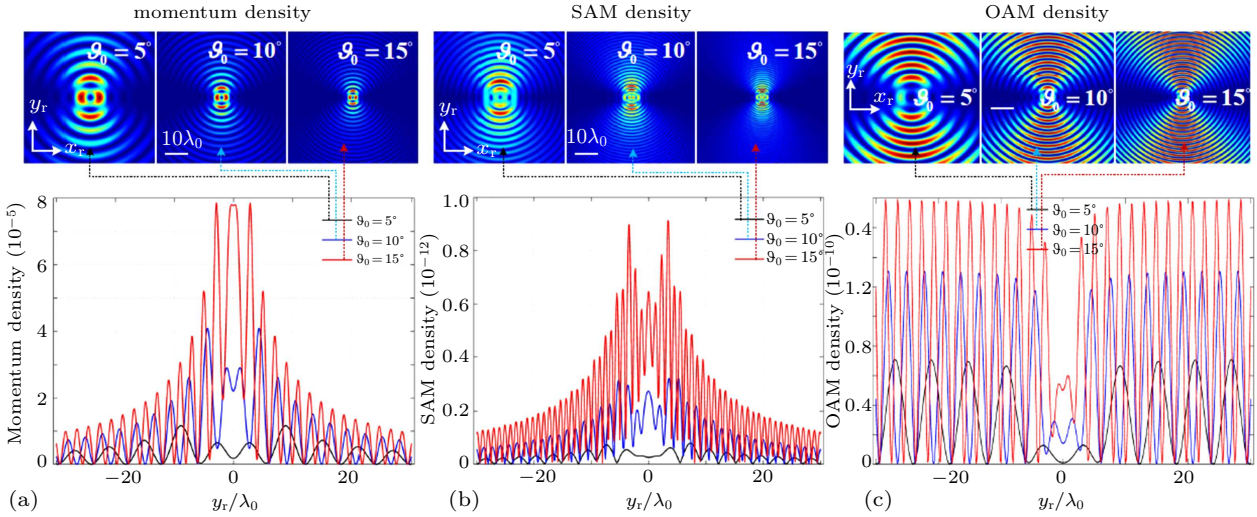


Fig. 5. Distributions of the momentum, SAM, and OAM densities of reflected Bessel beams with different half-cone angles. Panels (a)–(c) are the momentum, SAM, and OAM density distributions along $y_r(x_r = \lambda_0)$ axis in the x_r–y_r plane with half-cone angles $\vartheta_0 = 5°$, 10°, and 15°, respectively.

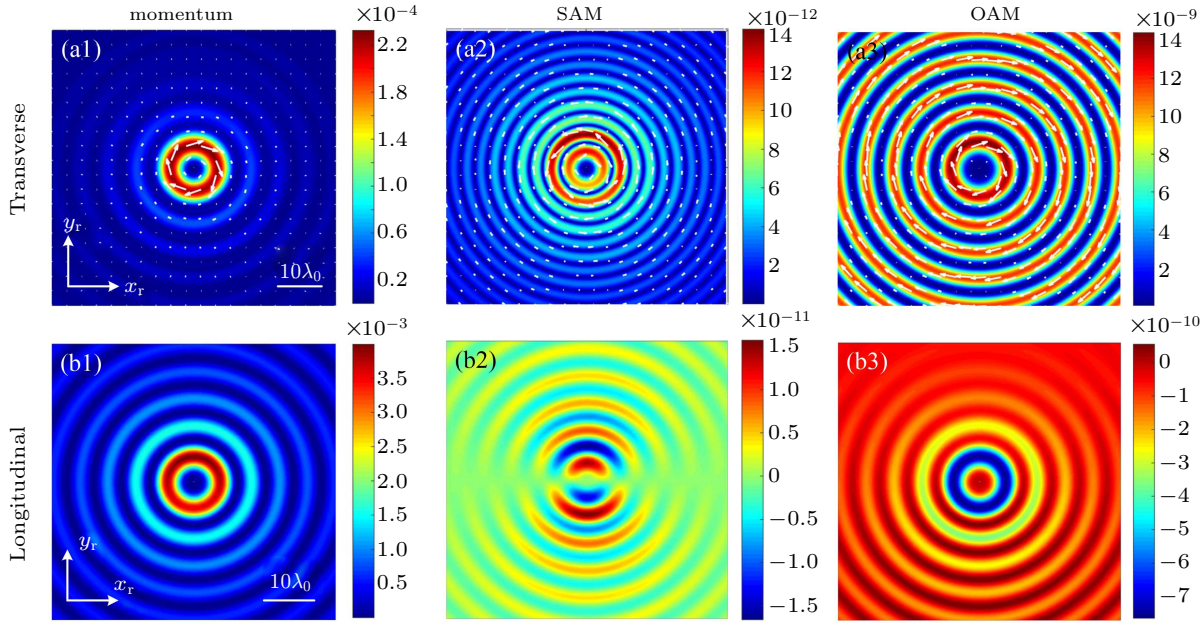


Fig. 6. Distributions of the transverse and longitudinal momentums, SAM, and OAM densities in the x_r–y_r plane for the Bessel beams with left circular polarization during the reflection process. (a1) and (b1) momentum, (a2) and (b2) SAM, (a3) and (b3) OAM, and the white arrows show the orientations of their corresponding transverse components.

4. Conclusion

In conclusion, we have investigated analytically and numerically the local dynamical characteristics of Bessel beams reflected from an air–glass interface near the Brewster angle. To describe such an issue exactly, a Taylor series expansion in form of angular spectrum component was applied to correct the reflection coefficients. The explicit analytical expressions for the electric and magnetic field components of the reflected Bessel beams were derived and used to calculate the energy,

momentum, SAM, and OAM. The effects of the incidence angle, topological charge, half-cone angle, and polarization state of the incident beams on these dynamical quantities are numerically simulated and discussed. The results show that the local dynamical characteristics of the Bessel beams during the reflection process at Brewster angle incidence change abruptly, and can be regulated by altering the sign and value of the topological charge, as well as the half-cone angle and polarization state. In particular, the change of the sign of the topological charge has a significant effect on the transverse momentum, and the longitudinal SAM and OAM, but has no effect on the longitudinal momentum, and the transverse SAM and OAM. As the topological charge increases, the profiles of these dynamical quantities gradually go away from the center. Meanwhile, with the increasing of half-cone angle, the distribution patters of these dynamical quantities gradually concentrate on the central area at the observation plane. In addition, with changing the polarization state of the incident beam from linear to circular, the corresponding momentum, transverse SAM, and OAM density distributions change from axisymmetric structure to multi ring structure. These findings are valuable in understanding the behavior of optical beams with vortex structure and diffraction-free nature during the reflection process, and have potential applications in the fields of optical sensing, information processing, and new optoelectronic devices design.

References

[1] Durnin J, Miceli J J and Eberly J H 1987 *Phys. Rev. Lett.* **58** 1499
[2] Bouchal Z 2003 *Czechoslovak Journal of Physics* **53** 537
[3] Ponomarenko S A, Huang W H and Cada M 2007 *Opt. Lett.* **32** 2508
[4] Yu X H, Yao B L, Lei M, Yan S H, Yang Y L, Li R Z and Cai Y N 2015 *Acta Phys. Sin.* **64** 244203 (in Chinese)
[5] Davis J A, Moreno I, Badham K, Sanchez-Lopez M M and Cottrell D M 2016 *Opt. Lett.* **41** 2270
[6] Rodriguez E S G, Machnoor M and Lazzi G 2017 *IEEE Trans. Anten. Propag.* **65** 5228
[7] Yang Z S, Zhang X, Bai C L and Wang M H 2018 *J. Opt. Soc. Am. A* **35** 452
[8] Cabrera-Rosas O D, Sosa-Sanchez C T, Julian-Macias I, Juarez-Reyes S A, Ortega-Vidals P, Espindola-Ramos E and Silva-Ortigoza G 2019 *J. Opt.* **21** 035603
[9] Chafiq A, Gouesbet G and Belafhal A 2020 *J. Quantum Spectrosc. Radiat. Transfer* **241** 106750
[10] Durnin J 1987 *J. Opt. Soc. Am. A* **4** 651
[11] Horvath Z L, Erdelyi M, Szabo G, Bor Z, Tittel F K and Cavallaro J R 1997 *J. Opt. Soc. Am. A* **14** 3009
[12] Chattrapiban N, Rogers E A, Cofield D, Hill W T and Roy R 2003 *Opt. Lett.* **28** 2183
[13] Martelli P, Tacca M, Gatto A, Moneta G and Martinelli M 2010 *Opt. Express* **18** 7108
[14] Gong L, Ren Y X, Xue G S, Wang Q C, Zhou J H, Zhong M C, Wang Z Q and Li Y M 2013 *Appl. Opt.* **52** 4566
[15] Du T J, Wang T and Wu F T 2013 *Acta Phys. Sin.* **62** 134103 (in Chinese)
[16] Moreno I, Davis J A, Sanchez-Lopez M M, Badham K and Cottrell D M 2015 *Opt. Lett.* **40** 5451
[17] Chen A T, Wang J J, Han Y P, Cui Z W and Yu M P 2018 *Opt. Express* **26** 26766
[18] Lai H M and Chan S W 2002 *Opt. Lett.* **27** 680
[19] Merano M, Aiello A, van Exter M P and Woerdman J P 2009 *Nat. Photon.* **3** 337
[20] Luo H L, Zhou X X, Shu W X, Wen S C and Fan D Y 2011 *Phys. Rev. A* **84** 043806
[21] Mugnai D 2002 *Opt. Commun.* **207** 95
[22] Novitsky A V and Barkovsky L M 2008 *J. Opt. Pure Appl. Opt.* **10** 075006
[23] Novitsky A V and Novitsky D V 2008 *Opt. Commun.* **281** 2727
[24] Aiello A and Woerdman J P 2011 *Opt. Lett.* **36** 543
[25] Brand?o P A and Pires D G 2017 *Phys. Lett. A* **381** 813
[26] Liu J W, Li H Y, Li R X, Bai L and Wu Z S 2020 *J. Quantum Spectrosc. Radiat. Transfer* **251** 107046
[27] Mugnai D 2013 *Opt. Commun.* **294** 17
[28] Volke-Sepulveda K, Garcés-Chávez V, Chávez-Cerda S, Arlt J and Dholakia K 2002 *J. Opt. B-Quantum Semiclass. Opt.* **4** S82
[29] Litvin I A, Dudley A and Forbes A 2011 *Opt. Express* **19** 16760
[30] Hernandez-Cedillo C L and Jauregui R 2011 *J. Opt.* **13** 064021
[31] Belyi V N, Khilo N A, Kurilkina S N and Kazak N S 2013 *J. Appl. Spectrosc.* **80** 458
[32] Belyi V N, Khilo N A, Kurilkina S N and Kazak N S 2013 *J. Opt.* **15** 044018
[33] Aleksanyan A and Brasselet E 2016 *Optica* **3** 167
[34] Nazarov S A, Gorbach D V, Mel'nikova E A, Kurilkina S N and Tolstik A L 2018 *J. Opt. Technol.* **85** 189
[35] Luo H, Zhou X, Shu W, Wen S and Fan D 2011 *Phys. Rev. A* **84** 043806
[36] Ritboon A, Croke S and Barnett S M 2019 *J. Opt. Soc. Am. B* **36** 482
[37] Bliokh K Y and Nori F 2015 *Phys. Rep.* **592** 1
[38] Bliokh K Y, Bekshaev A Y and Nori F 2017 *Phys. Rev. Lett.* **119** 073901
[39] Song P, Cui Z, Hui Y, Zhao W, Wang J and Han Y 2020 *J. Quantum Spectrosc. Radiat. Transfer* **241** 106715
[40] Erdelyi A, Magnus W and Oberhettinger F 1954 *Tables of integral transforms* (New York: McGraw-Hill)
[41] Luo H, Wen S, Shu W, Tang Z, Zou Y and Fan D 2009 *Phys. Rev. A* **80** 043810
[42] Luo H, Wen S, Shu W and Fan D 2010 *Phys. Rev. A* **82** 043825
[43] Qiu X, Zhang Z, Xie L, Qiu J, Gao F and Du J 2015 *Opt. Lett.* **40** 1018